Programmable Materials (2024), **2**:e6 1–10
doi:10.1017/pma.2024.4

PROGRAMMABLE MATERIALS

RESEARCH ARTICLE

Selective near-infrared laser programming for shape-memory polymer–carbon nanotube composite material 4D printing

Honggeng Li[1,2,3], Zhe Chen[1,2], Shouyi Yu[1,2], Bingcong Jian[1,2], Hanlin Yin[1,2] and Qi Ge[1,2]

[1]Shenzhen Key Laboratory of Soft Mechanics & Smart Manufacturing, Southern University of Science and Technology, Shenzhen, China.
[2]Department of Mechanical and Energy Engineering, Southern University of Science and Technology, Shenzhen, China.
[3]School of Advanced Engineering, Great Bay University, Dongguan, China.

Corresponding authors: Honggeng Li and Qi Ge; Email: lihonggeng@hnu.edu.cn, geq@sustech.edu.cn

H.L. and Z.C. contributed equally.

Received: 25 October 2023; **Revised:** 28 March 2024; **Accepted:** 9 April 2024

Keywords: 4D Printing; shape morphing; smart materials; light-responsive

Abstract

Light stimulation can realise the remote control of the deformation of the specific position of 4D printing structure. Shape-memory polymer–carbon nanotube (CNT) composite materials, with outstanding near-infrared photothermal conversion rate and shape-memory ability, is one type of the most popular light responsive smart materials. However, current studies focused on the photothermal effect and shape-memory applications of light-responsive shape-memory polymer composite (SMPC) sheet structures, and there is no research on the photothermal effect in the depth direction of light-responsive SMPC three-dimensional structures. Here, we prepared a UV curable, mechanically robust, and highly deformable shape-memory polymer (IBBA) as the matrix of light responsive SMPC. CNTs were added as photothermal conversion materials. We explore the photothermal effect of near-infrared laser on the surface and depth of IBBA–CNT composites cube. Shape-memory experiments show that different folded shapes can be obtained by selective near-infrared laser programming. Selective near-infrared laser programming three-dimensional movable type plate shows a programming application in depth direction of three-dimensional light-responsive intelligent structure. This research extends the application of near-infrared laser in 4D printing to the depth direction of intelligent structures, which will bring more complex and interesting 4D printing structures in the future.

Introduction

Shape-memory materials are intelligent materials that can transition from a temporary state to a primitive state under external stimuli. Compared with shape-memory materials such as hydrogels, liquid crystal elastomers, shape-memory alloys, and shape-memory ceramics, shape-memory polymers and their composites (SMPs/SMPCs) have the advantages of mechanical robustness, large deformability, low cost, easy preparation, and multiple stimulus actuation (Xiao Kuang et al., 2018). Stimulations such as light (Lendlein et al., 2005; Cortés et al., 2021; Liang et al., 2021), heat (Ge et al. 2013, 2014, 2016), electricity (Zarek et al., 2016; Zhang et al., 2021a, 2021b; Wang et al., 2023; Zhang et al., 2023), magnetism (Kim et al., 2018; Ma et al., 2020; Ze et al., 2020; Hu et al., 2021), pH (Han et al., 2012), and humidity (Sessini et al., 2018) can all be used to drive SMPs/SMPCs. The controllability of external stimulus such as heat/magnetic field/PH and humidity are poor, making it difficult to achieve quantitative driving deformation at specific locations. Dielectric elastomers cannot achieve specific position-driven deformation (Wang et al., 2023). Embedded conductors in the SMP structure can achieve electric heating at specific positions, but the driving position cannot be changed (Zarek et al., 2016; Zhang et al., 2021a; Zhang et al., 2023). Light stimulation can realise the remote control of the deformation of light-responsive SMPC structure at a specific position (Liang et al., 2021).

According to the deformation mechanism, light-responsive SMPC can be divided into photochemical type and photothermal type. Photochemical SMPC usually uses UV light or visible light to activate photochemical groups to form new chemical crosslinks, which leads to macro deformation of materials (Jin et al., 2018; Peng et al., 2021). This process is very slow (usually takes more than 1 hour), and the temporary deformation is unstable. Photothermal SMPC usually converts the energy of infrared light or sunlight into heat to drive the shape change (Leng et al., 2011; Wang et al., 2016; Wang et al., 2022). Photothermal SMPC usually has excellent shape fixation rate, shape recovery rate, and shape recovery speed, so it has been widely used in aerospace (Li et al., 2019b), medical devices (Xie et al., 2018; Chu et al., 2020; Yang et al., 2021), soft robots (Ji et al., 2014; Zhang et al., 2014; Ding et al., 2017; Toncheva et al., 2018; Xu et al., 2019; Wang et al., 2021; Shan et al., 2022), and self-healing SM structures (Li et al., 2019a; Du et al., 2020; Yan et al., 2020).

Common photothermal conversion materials include metal nanoparticles (Toncheva et al., 2018; Liang et al., 2021; Yang et al., 2021), carbon-based materials (Ji et al., 2014; Zhang et al., 2014; Ding et al., 2017; Li et al., 2019b; Wang et al., 2021), dyes (Fang et al., 2016), rare earths (Shan et al., 2022), and so forth. Carbon-based nanomaterials, that is, graphene (Ji et al., 2014)/carbon nanotubes (CNTs; Zhang et al., 2014; Ding et al., 2017)/carbon black (Wang et al., 2021, are the first choice of photothermal conversion materials due to their excellent photothermal conversion efficiency and good dispersion. CNTs are attractive for light-responsive SMPCs due to their excellent infrared light absorption and thermal conductivity (1,000–6,000 W/mK) (Kim et al., 2001; Liao et al., 2015; Han et al., 2018). Numerous studies have mixed CNT with shape-memory polymer matrix, such as thermoplastics (Zhang et al., 2014; Xu et al., 2019), PDMS elastomer (Li et al., 2018), and epoxy-based SMP, to prepare near-infrared activated SMPCs. However, the manufacturing methods of most matrix materials are injection moulding (Li et al., 2018), hot press moulding (Xu et al., 2019; Li et al., 2019a; Du et al., 2020), and vacuum filtration (Ding et al., 2017; Zhang et al., 2014), resulting in light-responsive SMPC structures being thin sheets. The combination of shape-memory polymer precursor solutions containing acrylic functional groups and 3D printing technology can produce structurally complex and functionally diverse light-responsive intelligent structures.

Here, we prepared a UV curable infrared responsive SMP–CNT composite material. Two monomers (IBoA, BA) and one crosslinker (aliphatic urethane diacrylate [AUD]) with acrylic functional groups form the UV curable SMP matrix (IBBA). This novel light-responsive SMPC (IBBA–CNT) was prepared by fully mixing IBBA with CNT. The thermal mechanical performance experiment, shape-memory effect experiment, and photothermal conversion experiment show that IBBA–CNT has good mechanical properties, shape-memory performance, and photothermal response performance. Selective near-infrared laser activation of specific regions of IBBA–CNT sheets can result in different folding structures. We explored the photothermal driving behaviour of near-infrared laser in the depth direction of light-responsive SMPC using 3D-printed IBBA–CNT cube. Based on the photothermal driving effect in the depth direction, we demonstrated the advantages of selective near-infrared light-driven three-dimensional SMP structures through a 3D-printed multi-material movable type.

Results and discussion

Figure 1a presents the chemical structures used to prepare the IBBA precursor solution which consists of 50 wt.% isobornyl acrylate (IBoA) and 30 wt.% benzyl acrylate (BA) as linear chain builder, 20 wt.% AUD as crosslinker. After the mixture of monomers and crosslinker is stirred and mixed evenly, add 2 wt.% diphenyl(2,4,6-trimethylbenzoly) phosphine oxide (TPO) as a photoinitiator. Light-responsive

https://doi.org/10.1017/pma.2024.4 Published online by Cambridge University Press

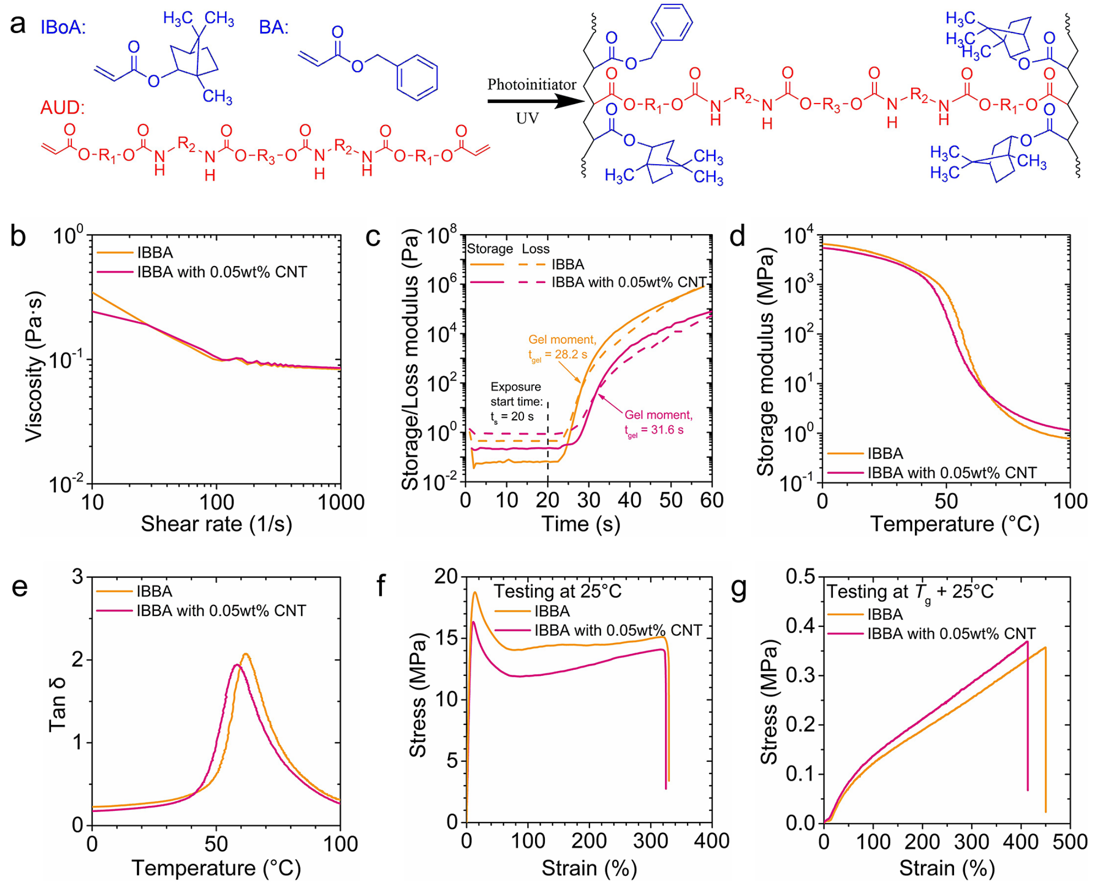

Figure 1. *The thermal mechanical properties and precursor rheological properties of IBBA–CNT. (a) Chemical composition and UV curing products of shape-memory polymer precursors. (b) The rheological properties of the precursors. (c) Photorheological properties of the precursors. (d,e) Dynamic thermodynamic performance test results. (f) Quasi-static tensile test results at room temperature. (g) Quasi-static tensile test results at programmed temperature.*

SMPC was prepared by adding 0.05 wt.% CNTs into IBBA solution and mixing them through ultrasound. After 30 min of ultrasonic mixing, the CNTs in IBBA–CNTs were uniformly dispersed and remained stationary for 12 h without significant precipitation. The addition of 0.05 wt.% CNTs has no significant effect on the rheological properties of IBBA precursor solution, and the viscosities are lower than 0.4 Pa·s before and after the addition of CNTs (Figure 1b, Supplementary Figure S1). The reduction of CNTs reduces the UV curing efficiency of IBBA precursor solution. The curing time of a 100-μm-thick IBBA–CNT layer is 11.6 s (UV light with an energy density of 8 mW/cm^2 and a wavelength of 385 nm, curing time: $t_c = t_{gel} - t_s$), which is much longer than the time required to cure an IBBA layer of the same thickness (Figure 1c).

We printed IBBA dog-bone samples and IBBA–CNT dog-bone samples to explore the effect of CNTs on the mechanical properties of IBBA (Supplementary Figure S1). DMA Q850 was used to measure their thermal mechanical properties (Figure 1d,e). The addition of 0.05 wt.% CNT reduced the glass modulus (storage modulus at room temperature) of IBBA and increased the rubbery modulus (storage modulus above the glass transition temperature) of IBBA. The addition of CNT also reduced the glass transition temperature (T_g) of the material (62° C to 58° C). During the DMA testing process, the temperature rises uniformly, and IBBA–CNT with higher thermal conductivity absorbs heat faster,

https://doi.org/10.1017/pma.2024.4 Published online by Cambridge University Press

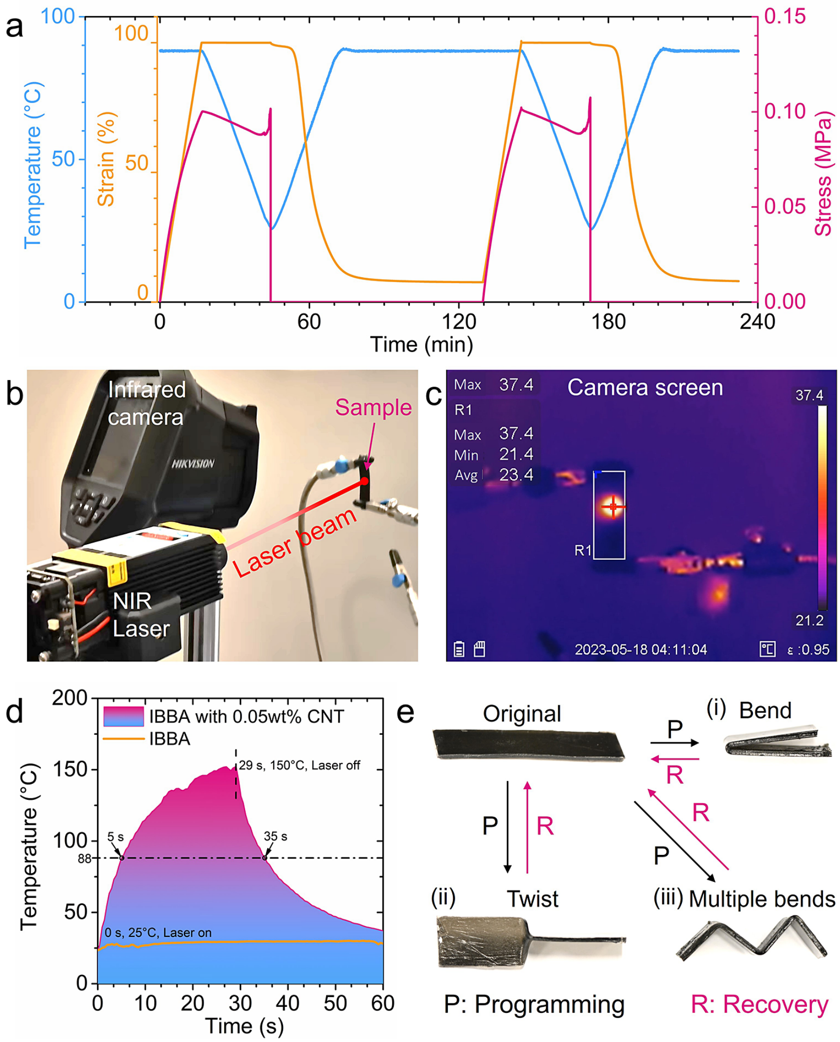

__Figure 2.__ Shape-memory programming of IBBA–CNT through near-infrared photothermal effects. (a) Shape-memory cycle experiment of IBBA–CNT. (b) Near-infrared photothermal effect testing equipment. (c) Infrared camera window. (d) Experimental results of near-infrared photothermal effect. (e) Selective near-infrared laser programming for IBBA–CNT sheet.

resulting in a lower measured glass transition temperature. The quasi-static tensile tests shown that the addition of CNT reduces the modulus of the material at room temperature (388 to 293 MPa; Figure 1f) and increases its modulus at programming temperature ($T_g + 25°$ C) (0.20 to 0.26 MPa; Figure 1g), but has no significant effect on the elongation at break of the materials (450.1% to 413.6%; Figure 1g). The test results of thermal mechanical properties show that the addition of CNT has a significant effect on the strength of the material, but the material still has a high modulus at room temperature and maintains a large deformation capacity at programming temperature.

The shape-memory experiment and near-infrared laser thermal effect experiment demonstrate that IBBA–CNT is an excellent light-responsive SMPC. Figure 2a shows two shape-memory cycles of IBBA–CNT. The shape fixation rates in two shape-memory cycles are all 99.9%. The shape recovery rate of the first cycle is 89.8%, and after training in the first cycle, the shape recovery rate of the second cycle is 99.8%. The testing device for the surface photothermal effect of IBBA–CNT is shown

https://doi.org/10.1017/pma.2024.4 Published online by Cambridge University Press

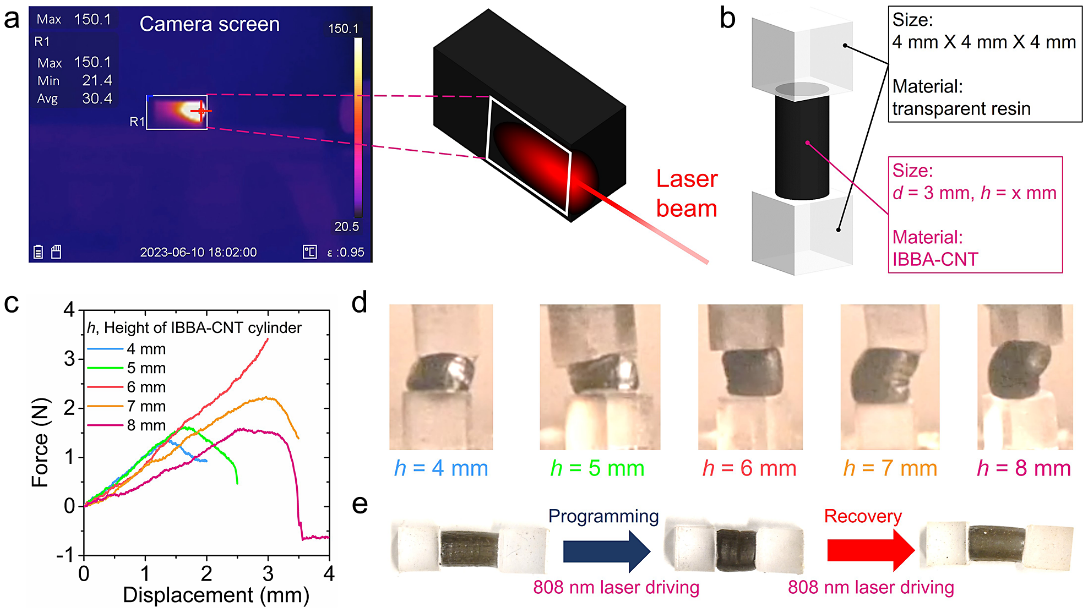

Figure 3. *Near-infrared laser programming for IBBA–CNT three-dimensional pillar. (a) Experimental schematic diagram of the effective thermal response depth of near-infrared laser on IBBA–CNT. (b) Design drawing of a three-dimensional multi-material pillar. (c) Compression experiments of three-dimensional multi-material pillars with different heights at programming temperature. (d) Snapshots of 50% compressive strain of three-dimensional multi-material pillars. (e) Near-infrared laser programming for 3D multi-material pillar.*

in Figure 2b. The infrared camera records the temperature changes of IBBA–CNT sheet irradiated by near-infrared laser. Figure 2c shows the screen of an infrared camera, which can only record the temperature changes of the IBBA–CNT sheet without recording the surrounding environment by adjusting the temperature measurement range (white rectangular box in the centre of the screen). The surface temperature variation curve of IBBA–CNT sheet (Figure 2d) was plotted based on the infrared camera video during the experimental process. Due to the excellent photothermal effect of CNT, near-infrared laser can rapidly heat IBBA–CNT, reaching the programming temperature (88° C) in just 5 s and 150° C in just 29 s. After reaching 150° C, turn off the laser, and the IBBA–CNT sheet rapidly cools to the programming temperature (6 s), and then slowly cools to room temperature. To achieve programming of IBBA–CNT sheets, it is necessary to irradiate at a specific position for more than 5 s and quickly complete the programming operation within 6 s after turning off the laser.

We demonstrated the selective region activation and programming of the IBBA–CNT sheet by near-infrared laser, as well as the selective region activation and recovery (Figure 2e). After selectively irradiating the centre of the sheet, both bending and twisting deformations can be completed (Figure 2e(i,ii)). After selectively irradiating multiple areas, bending deformation can be achieved at multiple locations in the sheet to form an ‘M’ shape (Figure 2e(iii)), and controllable sequential recovery can be achieved through selective near-infrared laser irradiation (in Supplementary Video S1, the left bend of the ‘M’-shaped sheet is first unfolded, then the right bend is unfolded, and finally the middle bend is unfolded).

Further, 0.05 wt.% CNT not only endows IBBA shape-memory polymers with the ability to respond to near-infrared laser, but also enables near-infrared laser transmission to a certain depth in the material. This will endow the material with near-infrared laser response capability in the depth direction, which has not been addressed in previous work. We tested the near-infrared photothermal depth influence range of IBBA–CNT (0.05 wt.% CNT) using the method shown in Figure 3a. As shown in Figure 3a,

https://doi.org/10.1017/pma.2024.4 Published online by Cambridge University Press

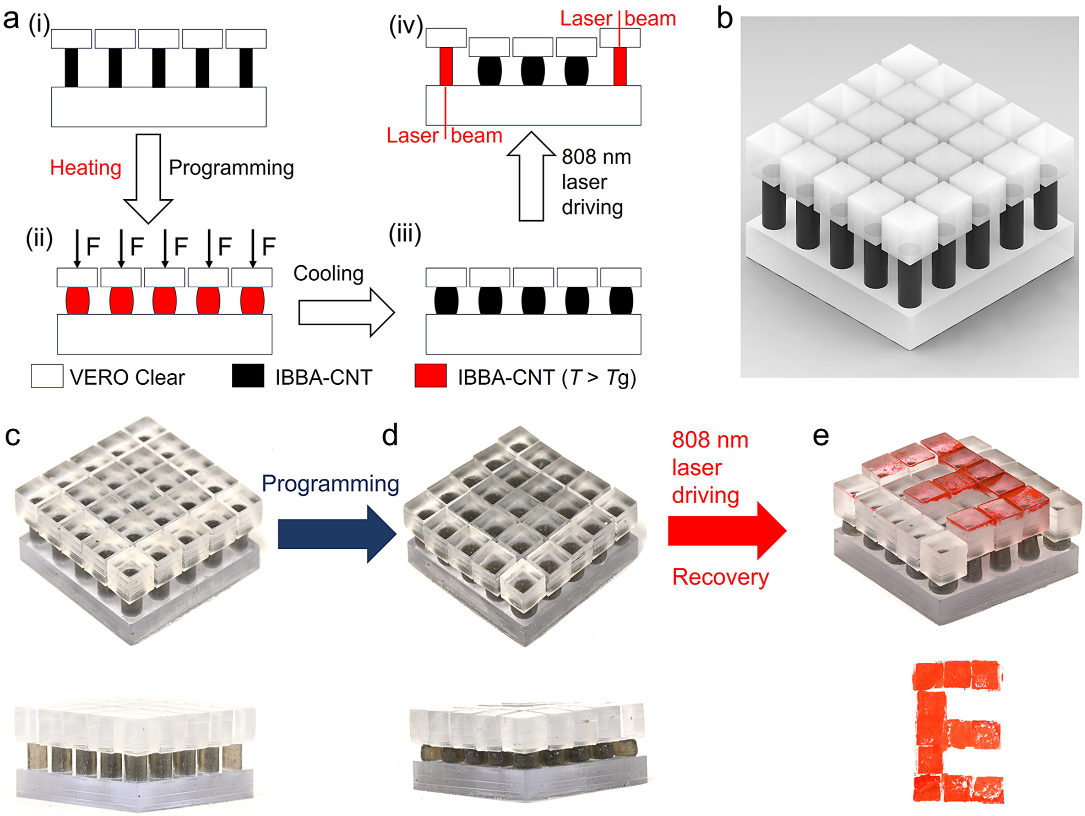

Figure 4. *Selective near-infrared laser programming for IBBA–CNT shape-memory movable type plate 4D printing. (a) Schematic diagram of selective infrared laser programming movable type plate. (b) Digital model of multi-material movable type plate. (c) DLP 3D-printed model of multi-material movable type plate. (d) Movable type plate in compressed state. (e) Movable type 'E' obtained by selective near-infrared laser programming.*

a near-infrared laser is irradiated on the edge of the right side of the 3D-printed IBBA–CNT cube, and the infrared camera records the temperature changes on the front face of the cube. When the maximum temperature reaches 150° C, turn off the near-infrared laser and record the infrared camera image at this moment. Based on the temperature scale and the size of the cube, we measured the size of the area where the temperature on the front face of the cube exceeded 88° C. This area is called an effectively programmable heat affected zone, with a length of approximately 8 mm and a width exceeding 8 mm. This provides design parameters for the design of three-dimensional IBBA–CNT structures.

As shown in Figure 3b, we design three-dimensional multi-material pillars with 3D-printed transparent photocurable resin material at both ends (cubes with a side length of 4 mm) and 3D-printed IBBA–CNT cylinder in the middle (diameter: $d = 3$ mm, heights: $h = 4, 5, 6, 7$, or 8 mm). Figure 3c depicts the force displacement curve of compressing three-dimensional multi-material pillars with different heights to 50% strain at a strain rate of 0.01 s^{-1} at programming temperature. Under 50% compressive strain, the 4- and 5-mm-high IBBA–CNT cylinders showed significant barrelling deformation and creasing, and the 7- and 8-mm-high cylinders showed significant buckling and creasing. However, the 6-mm column has barrelling deformation and small creases under 50% compressive strain (Figure 3d). Therefore, a diameter of 3 mm and a height of 6 mm are ideal designs for IBBA–CNT cylinders. Figure 3e illustrates the shape-memory experiment of IBBA–CNT cylinder with $h = 6$ mm. Under the photothermal effect of near-infrared laser, the IBBA–CNT cylinder is compressed and programmed. After turning off the

https://doi.org/10.1017/pma.2024.4 Published online by Cambridge University Press

laser, the material quickly cools and the compressed shape is fixed. The IBBA–CNT cylinder freely recovers to its initial height by turning on the near-infrared laser again.

Multiple multi-material 3D pillars are combined to form a movable type plate, and different printing movable types can be obtained through selective infrared laser programming. The schematic diagram of the selective infrared laser programming movable type board is shown in Figure 4a. The side view of the multi-material 3D-printed movable type plate is shown in Figure 4a(i). After heating to the programming temperature, the height of the IBBA–CNT cylinders decreases after external force compression (Figure 4a(ii)). Maintain the compressed state and cool to room temperature, and the movable type plate is locked in a flat shape (Figure 4a(iii)). Near-infrared laser can penetrate the transparent resin at both ends of the pillars and directly irradiate the IBBA–CNT cylinders. The IBBA–CNT cylinders activated by photothermal activation can be freely restored to their original height (Figure 4a(iv)). Figure 4b,c shows the digital model and 3D printing model of movable type plate composed of five rows and five columns of multi-material pillars, respectively. Figure 4d shows a movable type plate programmed to a compressed flat state. Selective near-infrared laser irradiation of the pillars can decode the flat-shaped movable type plate to form the required upward protruding movable type (Figure 4e and Supplementary Video S2).

Conclusion

We have developed a near-infrared responsive SMPC material, IBBA–CNT, with high mechanical strength, strong deformation ability, and UV curability. It can be used to produce near-infrared-driven 4D printing structures through digital light processing. IBBA–CNT containing 0.05 wt.% CNT has good shape-memory performance and photothermal effect: shape fixation rate is 99.9%, shape recovery rate is 99.8%, and programming temperature can be reached after 5 s of irradiation with a 250-mW 808-nm near-infrared laser. We demonstrated the selective near-infrared laser programming of IBBA–CNT sheets into various origami and their recovery process in a controllable sequence. More importantly, for the first time, we explored the photothermal effect of near-infrared laser in the depth direction of light-responsive SMP. We printed IBBA–CNT multi-material pillars and conducted experiments to demonstrate the feasibility of near-infrared laser programming in the depth direction. Finally, we designed a movable type board to demonstrate the application of selective near-infrared laser programming in deep direction activation of light-responsive SMPC. It can be predicted that there will be more research on the design and application of three-dimensional light-responsive SMPC structure in the future.

Materials and methods

Materials

Isobornyl arcylate (IBoA), Benzyl acrylate (BA), diphenyl(2,4,6-trimethylbenzoly) phosphine oxide (TPO) were purchased from Sigma-Aldrich (Shanghai, China). CNTs were purchased from XFNANO (Nanjing, China). Ebecryl 8413 (AUD) was kindly provided by Allnex (Frankfurt am Main, Germany).

Rheological test

The viscosity (η) of IBBA and IBBA–CNT precursors were measured by using a controlled-stress rheometer (DHR2, TA Instruments, Inc., Elstree, UK) with an aluminium plate geometry (diameter 25 mm, gap 100 μm).

Photorheological test

The storage modulus and loss modulus of materials were measured on a DHR2 machine with an aluminium plate geometry (diameter 20 mm, gap 100 μm). First, 20 s were detected without light, then

20 s were exposed in 385-nm UV light with 8-mW/cm^2 light intensity, and more 20 s were detected after the end of exposure. Aluminium plate rotated at a speed of 5 rad s^{-1} throughout the 60-s detection process. The intersection of the loss modulus and storage modulus curves is the gel point, and the corresponding time minus 20 s is the curing time.

Dynamic mechanical analysis experiments

Samples with dimensions of 10 mm × 5 mm × 1 mm were tested at a frequency of 1 Hz and an amplitude of 10 μm using a DMA analyser (Q850 DMA, TA Instruments). The temperature was first equilibrated at −20° C for 3 min, and then gradually increased to 100° C at a heating rate of 3° C/min. The glass transition temperatures (T_g) were assigned as the temperature at which tanδ value was maximum.

Uniaxial tensile experiments

Tension experiments on dog-bone samples with a gauge length of 20 mm and a cross section of 5 mm × 2 mm were conducted using MTS machine at a strain rate of 0.01 s^{-1}.

Shape-memory behaviour tests

Figure 2a presents the result from typical shape-memory cyclic tests for calculating shape fixation ratio ($R_f = \varepsilon_u/\varepsilon_p$) and shape recovery ratio ($R_r = (\varepsilon_u - \varepsilon_r)/\varepsilon_u$). First, an IBBA–CNT sample is stretched to 100% at a constant strain rate (0.001 s^{-1}) at T_g + 25° C (88° C). Second, the sample is cooled to 25° C (−2.5° C/min) and held 2 min while it is kept stretched. Third, the external load is suddenly released at 25° C, and the temporary fixed strain ε_u can be measured. Last, the sample is heated to T_g + 25° C (2.5° C/min) and held at T_g + 25° C for 1 h where the recovery strain ε_r is measured.

3D printing

A self-assembled multi-materials DLP printer (Cheng et al., 2022) was used to print multi-materials structures. The slice thickness of IBBA–CNT layers is 100 μm, and the exposure time of each layer is 12 s (exposure intensity 8 mW/cm^2).

Supplementary material. The supplementary material for this article can be found at http://doi.org/10.1017/pma.2024.4.

Data availability statement. The data that support the findings of this study are available from the first author and the corresponding author upon reasonable request.

Funding statement. This work was supported by the National Natural Science Foundation of China (H.L.; Grant No. 52305312), the Natural Science Foundation of Guangdong Province (H.L.; Grant No. 2022A1515010047), the Science, Technology Innovation Program of the Ministry of Trade, Industry & Energy (MOTIE, Korea) (Q.G.; Grant No. 20009618), and the Technology and Innovation Commission of Shenzhen Municipality (Q.G.; Grant No. ZDSYS20210623092005017).

Competing interest. The authors declare none.

Author contributions. Q.G. and H.L. conceived and designed the study. H.L. and Z.C. conducted experiments with assistance from S.Y., B.J. and H.Y. H.L. and Z.C. conducted data analyses. H.L., Z.C. and Q.G. wrote the article.

References

Cheng J, **Wang R**, **Sun Z**, **Liu Q**, **He X**, **Li H**, **Ye H**, **Yang X**, **Wei X**, **Li Z**, **Jian B**, **Deng W** and **Ge Q** (2022) Centrifugal multimaterial 3D printing of multifunctional heterogeneous objects. *Nature Communications* **13**(1), 7931. https://doi.org/10.1038/s41467-022-35622-6

Chu C, **Xiang Z**, **Wang J**, **Xie H**, **Xiang T** and **Zhou S** (2020) A near-infrared light-triggered shape-memory polymer for long-time fluorescence imaging in deep tissues. *Journal of Materials Chemistry B* **8**(35), 8061–8070.

Cortés A, **Cosola A**, **Sangermano M**, **Campo M**, **González Prolongo S**, **Pirri CF**, **Jiménez-Suárez A** and **Chiappone A** (2021) DLP 4D-printing of remotely, modularly, and selectively controllable shape memory polymer nanocomposites embedding carbon nanotubes. *Advanced Functional Materials* **31**(50), 2106774. https://doi.org/10.1002/adfm.202106774

Ding Z, **Yuan C**, **Peng X**, **Wang T**, **Qi HJ** and **Dunn ML** (2017) Direct 4D printing via active composite materials. *Science Advances* **3**(4), e1602890.

Du W, **Jin Y**, **Shi L**, **Shen Y**, **Lai S** and **Zhou Y** (2020) NIR-light-induced thermoset shape memory polyurethane composites with self-healing and recyclable functionalities. *Composites Part B: Engineering* **195**, 108092. https://doi.org/10.1016/j.compositesb.2020.108092

Fang L, **Fang T**, **Liu X**, **Chen S**, **Lu C** and **Xu Z** (2016) Near-infrared light triggered soft actuators in aqueous media prepared from shape-memory polymer composites. *Macromolecular Materials and Engineering* **301**(9), 1111–1120. https://doi.org/10.1002/mame.201600139

Ge Q, **Dunn CK**, **Qi HJ** and **Dunn ML** (2014) Active origami by 4D printing. *Smart Materials and Structures* **23**(9), 094007. https://doi.org/10.1088/0964-1726/23/9/094007

Ge Q, **Qi HJ** and **Dunn ML** (2013) Active materials by four-dimension printing. *Applied Physics Letters* **103**(13), 131901.

Ge Q, **Sakhaei AH**, **Lee H**, **Dunn CK**, **Fang NX** and **Dunn ML** (2016) Multimaterial 4D printing with tailorable shape memory polymers. *Scientific Reports* **6**, 31110. https://doi.org/10.1038/srep31110

Han XJ, **Dong ZQ**, **Fan MM**, **Liu Y**, **li JH**, **Wang YF**, **Yuan Q-J**, **Li B-J** and **Zhang S** (2012) pH-induced shape-memory polymers. *Macromolecular Rapid Communications* **33**(12), 1055–1060. https://doi.org/10.1002/marc.201200153

Han B, **Zhang YL**, **Chen QD** and **Sun HB** (2018) Carbon-based Photothermal actuators. *Advanced Functional Materials* **28**(40), 1802235. https://doi.org/10.1002/adfm.201802235

Hu X, **Yasa IC**, **Ren Z**, **Goudu SR**, **Ceylan H**, **Hu W** and **Sitti M** (2021) Magnetic soft micromachines made of linked microactuator networks. *Science Advances* **7**(23), eabe8436.

Ji M, **Jiang N**, **Chang J** and **Sun J** (2014) Near-infrared light-driven, highly efficient bilayer actuators based on polydopamine-modified reduced graphene oxide. *Advanced Functional Materials* **24**(34), 5412–5419. https://doi.org/10.1002/adfm.201401011

Jin B, **Song H**, **Jiang R**, **Song J**, **Zhao Q** and **Xie T** (2018) Programming a crystalline shape memory polymer network with thermo- and photo-reversible bonds toward a single-component soft robot. *Science Advances* **4**(1), eaao3865. https://doi.org/10.1126/sciadv.aao3865

Kim P, **Shi L**, **Majumdar A** and **McEuen PL** (2001) Thermal transport measurements of individual multiwalled nanotubes. *Physical Review Letters* **87**(21), 215502. https://doi.org/10.1103/PhysRevLett.87.215502

Kim Y, **Yuk H**, **Zhao R**, **Chester SA** and **Zhao X** (2018) Printing ferromagnetic domains for untethered fast-transforming soft materials. *Nature* **558**(7709), 274–279. https://doi.org/10.1038/s41586-018-0185-0

Lendlein A, **Jiang H**, **Jünger O** and **Langer R** (2005) Light-induced shape-memory polymers. *Nature* **434**(7035), 879–882.

Leng J, **Lan X**, **Liu Y** and **Du S** (2011) Shape-memory polymers and their composites: Stimulus methods and applications. *Progress in Materials Science* **56**(7), 1077–1135. https://doi.org/10.1016/j.pmatsci.2011.03.001

Li F, **Hou H**, **Yin J** and **Jiang X** (2018) Near-infrared light-responsive dynamic wrinkle patterns. *Science Advances* **4**(4), eaar5762.

Li T, **Li Y**, **Wang X**, **Li X** and **Sun J** (2019a) Thermally and near-infrared light-induced shape memory polymers capable of healing mechanical damage and fatigued shape memory function. *ACS Applied Materials & Interfaces* **11**(9), 9470–9477. https://doi.org/10.1021/acsami.8b21970

Li F, **Liu L**, **Lan X**, **Pan C**, **Liu Y**, **Leng J** and **Xie Q** (2019b) Ground and geostationary orbital qualification of a sunlight-stimulated substrate based on shape memory polymer composite. *Smart Materials and Structures* **28**(7), 075023.

Liang R, **Yu H**, **Wang L**, **Wang N** and **Amin BU** (2021) NIR light-triggered shape memory polymers based on mussel-inspired iron–catechol complexes. *Advanced Functional Materials* **31**(32), 2102621. https://doi.org/10.1002/adfm.202102621

Liao Q, **Liu Z**, **Liu W**, **Deng C** and **Yang N** (2015) Extremely high thermal conductivity of aligned carbon nanotube–polyethylene composites. *Scientific Reports* **5**, 16543. https://doi.org/10.1038/srep16543

Ma C, **Wu S**, **Ze Q**, **Kuang X**, **Zhang R**, **Qi HJ** and **Zhao R** (2020) Magnetic multimaterial printing for multimodal shape transformation with tunable properties and shiftable mechanical behaviors. *ACS Applied Materials & Interfaces* **13**(11), 12639–12648. https://doi.org/10.1021/acsami.0c13863

Peng W, **Zhang G**, **Zhao Q** and **Xie T** (2021) Autonomous off-equilibrium morphing pathways of a supramolecular shape-memory polymer. *Advanced Materials* **33**(34), e2102473. https://doi.org/10.1002/adma.202102473

Sessini V, **Arrieta MP**, **Fernandez-Torres A** and **Peponi L** (2018) Humidity-activated shape memory effect on plasticized starch-based biomaterials. *Carbohydrate Polymers* **179**, 93–99. https://doi.org/10.1016/j.carbpol.2017.09.070

Shan P, **Chen X**, **Tan B**, **Cao D**, **Fang L**, **Lu C** and **Xu Z** (2022) Uniform contraction and high force output of photoresponsive shape-memory polymer actuators with large thickness based on vertical distribution of rare earth oxides. *Macromolecular Materials and Engineering* **307**(3), 2100683.

Toncheva A, **Khelifa F**, **Paint Y**, **Voue M**, **Lambert P**, **Dubois P** and **Raquez JM** (2018) Fast IR-actuated shape-memory polymers using in situ silver nanoparticle-grafted cellulose nanocrystals. *ACS Applied Materials & Interfaces* **10**(35), 29933–29942. https://doi.org/10.1021/acsami.8b10159

Wang W, **Liu Y** and **Leng J** (2016) Recent developments in shape memory polymer nanocomposites: Actuation methods and mechanisms. *Coordination Chemistry Reviews* **320 –321**, 38–52. https://doi.org/10.1016/j.ccr.2016.03.007

Wang Y, **Wang Y**, **Wei Q** and **Zhang J** (2022) Light-responsive shape memory polymer composites. *European Polymer Journal* **173**, 111314. https://doi.org/10.1016/j.eurpolymj.2022.111314

Wang D, **Zhao B**, **Li X**, **Dong L**, **Zhang M**, **Zou J** and **Gu G** (2023) Dexterous electrical-driven soft robots with reconfigurable chiral-lattice foot design. *Nature Communications* **14**(1), 5067. https://doi.org/10.1038/s41467-023-40626-x

Wang T, **Zhao J**, **Weng C**, **Wang T**, **Liu Y**, **Han Z** and **Zhang Z** (2021) A bidirectionally reversible light-responsive actuator based on shape memory polyurethane bilayer. *Composites Part A: Applied Science and Manufacturing* **144**, 106322. https://doi.org/10.1016/j.compositesa.2021.106322

Xiao Kuang DJR, **Wu J**, **Hamel CM**, **Ding Z**, **Wang T**, **Dunn ML** and **Qi HJ** (2018) Advances in 4D printing: Materials and applications. *Advanced Functional Materials* **29**, 1805290. https://doi.org/10.1002/adfm.afdm201805290

Xie H, **Shao J**, **Ma Y**, **Wang J**, **Huang H**, **Yang N**, **Wang H**, **Ruan C**, **Luo Y**, **Wang Q-Q**, **Chu PK** and **Yu XF** (2018) Biodegradable near-infrared-photoresponsive shape memory implants based on black phosphorus nanofillers. *Biomaterials* **164**, 11–21. https://doi.org/10.1016/j.biomaterials.2018.02.040

Xu Z, **Ding C**, **Wei DW**, **Bao RY**, **Ke K**, **Liu Z**, **Yang M-B** and **Yang W** (2019) Electro and light-active actuators based on reversible shape-memory polymer composites with segregated conductive networks. *ACS Applied Materials & Interfaces* **11**(33), 30332–30340. https://doi.org/10.1021/acsami.9b10386

Yan J, **Li M**, **Wang Z**, **Chen C**, **Ma C** and **Yang G** (2020) Highly tough, multi-stimuli-responsive, and fast self-healing supramolecular networks toward strain sensor application. *Chemical Engineering Journal* **389**, 123468. https://doi.org/10.1016/j.cej.2019.123468

Yang C, **Zheng R**, **Younis MR**, **Shao J**, **Fu L-H**, **Zhang D-Y**, **Lin J**, **Li Z** and **Huang P** (2021) NIR-II light-responsive biodegradable shape memory composites based on cuprorivaite nanosheets for enhanced tissue reconstruction. *Chemical Engineering Journal* **419**, 129437. https://doi.org/10.1016/j.cej.2021.129437

Zarek M, **Layani M**, **Cooperstein I**, **Sachyani E**, **Cohn D** and **Magdassi S** (2016) 3D printing of shape memory polymers for flexible electronic devices. *Advanced Materials* **28**(22), 4449–4454. https://doi.org/10.1002/adma.201503132

Ze Q, **Kuang X**, **Wu S**, **Wong J**, **Montgomery SM**, **Zhang R**, **Kovitz JM**, **Yang F**, **Qi HJ** and **Zhao R** (2020) Magnetic shape memory polymers with integrated multifunctional shape manipulation. *Advanced Materials* **32**(4), 1906657.

Zhang B, **Li H**, **Cheng J**, **Ye H**, **Sakhaei AH**, **Yuan C**, **Rao P**, **Zhang Y-F**, **Chen Z**, **Wang R**, **He X**, **Liu J**, **Xiao R**, **Qu S** and **Ge Q** (2021a) Mechanically robust and UV-curable shape-memory polymers for digital light processing based 4D printing. *Advanced Materials* **33**(27), e2101298. https://doi.org/10.1002/adma.202101298

Zhang YF, **Li Z**, **Li H**, **Li H**, **Xiong Y**, **Zhu X**, **Lan H** and **Ge Q** (2021b) Fractal-based stretchable circuits via electric-field-driven microscale 3D printing for localized heating of shape memory polymers in 4D printing. *ACS Applied Materials & Interfaces* **13**(35), 41414–41423. https://doi.org/10.1021/acsami.1c03572

Zhang Y-F, **Li H**, **Long C**, **Xiong Y** and **Ge Q** (2023) Tailorable activation of thermoresponsive composite structures incorporating wavy heaters via hybrid manufacturing. *Composites Communications* **38**, 101523.

Zhang X, **Yu Z**, **Wang C**, **Zarrouk D**, **Seo JW**, **Cheng JC**, **Buchan AD**, **Takei K**, **Zhao Y**, **Ager JW**, **Zhang J**, **Hettick M**, **Hersam MC**, **Pisano AP**, **Fearing RS** and **Javey A** (2014) Photoactuators and motors based on carbon nanotubes with selective chirality distributions. *Nature Communications* **5**, 2983. https://doi.org/10.1038/ncomms3983

Cite this article: Li, H., Chen, Z., Yu, S., Jian, B., Yin, H., and Ge, Q. (2024). Selective near-infrared laser programming for shape-memory polymer–carbon nanotube composite material 4D printing. *Programmable Materials*, **2**, e6. https://doi.org/10.1017/pma.2024.4